ACS OMEGA

Article

Cite This: ACS Omega 2017, 2, 8388−8400

Effect of Water Interactions on Polyvinylamine at Different pHs for Membrane Gas Separation

Daniel Romero Nieto, Arne Lindbråthen, and May-Britt Hägg*

Department of Chemical Engineering, Norwegian University of Science and Technology, N-7491 Trondheim, Norway

Supporting Information

ABSTRACT: In our previous work, it was shown that the separation performance of the fixed-site-carrier polyvinylamine (PVAm) composite membrane increases exponentially with increasing relative humidity content in the gas. Through these efforts, it has been important to develop a greater understanding of the relationship between the water, structural, and interfacial properties of the PVAm surface. The degree of hydrophilicity of a given surface plays a crucial role in the separation performance of the membrane when exposed to a humidified gas. Therefore, in the current work, the wettability properties of PVAm at different pHs have been studied by experimental measurements and molecular dynamic simulations. It was confirmed that the intramolecular interactions are not linearly dependent on pH. As well as the H-bonding between protonated and unprotonated amine groups, the conformation polymer chain and the distribution charge density play a crucial role in the surface stability and wettability properties.

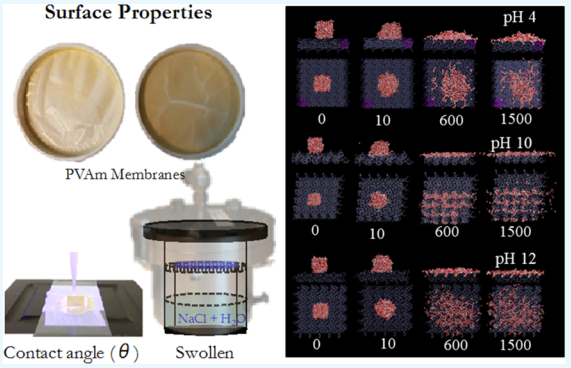

1. INTRODUCTION

Polyvinylamine (PVAm) is a linear polyelectrolyte type of polymer, which is water-soluble with high contents of primary amine and thereby high ion content. Measurements have revealed contents as high as 19 meq/g polymer.[1] The amine groups in the polymer are flexible and may function as reaction sites, thus the polymer becomes very attractive as a functional polymer having a variety of hydrophobic/hydrophilic properties at the macroscopic surface/interface.[2] Furthermore, PVAm is highly pH sensitive, which enables the polymer to be stimuli-responsive.[3−5] PVAm has been synthesized following different routes.[6,7] However, from polyacrylamide by the Hofmann reaction[8] is the most used route. High molecular weight PVAm can also be obtained commercially.

PVAm is an attractive polymer to use in different fields, including biomedical applications,[9] encapsulation,[10,11] oil recovery,[12] and especially, it has been extensively studied as a fixed-site-carrier polyvinylamine membrane for carbon dioxide capture where a thin selective layer of PVAm is deposited on a polysulfone support. These membranes[13−25] have been reported both as composite flat sheets and hollow fiber membranes.[26,27] One of the reasons for its success is because the PVAm coating on the membrane acts as the transport medium for the CO_2 in humidified gas. The amine group performs as the carrier of the CO_2, increasing the transport performance of the membrane by facilitating the reaction taking place in addition to the conventional solution-diffusion mechanism. PVAm composite membranes in dry conditions will separate according to a solution-diffusion mechanism only. It was documented by Kim et al. in 2004[8] that by allowing the membrane to be exposed to gas with high relative humidity, the separation performance increased exponentially.[8,22,26] It is, however, important to develop a more comprehensive understanding of the relationships between the structure and the interfacial properties of the PVAm−water surface. The degree of hydrophilicity of a given surface requires an understanding of the microscale principles that, in turn, control the macroscale surface-wetting behavior. Moreover, all of these applications are possible because of the adsorbing potential of the PVAm surface with water and the pH-dependent polycationic nature of PVAm.[28] Hence, to use PVAm as a membrane for separation of selected gas components, the amine groups in the polymer must preferably be unprotonated for them to be available to promote the facilitated transport of selected gas components (i.e., CO_2). It is therefore of vital importance to understand the impact of water and pH on the separation performance.

Studies based on molecular modeling should, in principle, offer help on an atomistic level for understanding these interactions and therefore establish a theoretical tool to predict the relevant technological parameter values. In the current work, these PVAm−water interactions were studied at the nanoscale level, both by experimental measurements and molecular modeling. The molecular dynamic simulations contribute to an understanding of the inter−intramolecular interactions and moreover of the transport mechanism giving

Received: September 5, 2017
Accepted: November 2, 2017
Published: November 29, 2017

DOI: 10.1021/acsomega.7b01307
ACS Omega 2017, 2, 8388−8400

the possibility to estimate the related technological parameter values.

2. EXPERIMENTAL WORK

2.1. Membrane Preparation. The membrane was prepared by casting a pH-adjusted 3 wt % PVAm solution onto a Teflon plate.[8,26] Casting solutions of pHs 4, 10, and 12 were used. The desired thickness of PVAm was controlled by pouring a known volume of solution into a confined circular Teflon mold with known surface area. The resulting PVAm thickness was 20 μm on a dry basis for all membranes. The membranes were dried at 45 °C and kept at room temperature for 24 h, they were then deep dried at 90 °C for 1 h, and finally cooled down in the oven for 1 h. The thickness of the dry membranes was confirmed by several measurements randomly distributed across the membrane using a micrometer Digitrisk II NSK (0.001−25 mm).

Because of the low mechanical strength of the PVAm membrane when cast as a stand-alone selective layer, defects may appear during the preparation. For this reason, performing permeation tests in dry and wet (relative humidity RH%) conditions was very challenging.

2.2. Swelling Test. The swelling performance of the PVAm membrane under different humid conditions at room temperature was measured. The samples of PVAm of pHs 4, 10, and 12, which were cast into films on the Teflon plate, were placed in a hydrophobic plastic Petri dish and mounted into a closed humidity chamber. Beneath the polymer film, different saturated salt solutions were added but not in direct contact with the polymer, see Figure 1; the solutions used were all

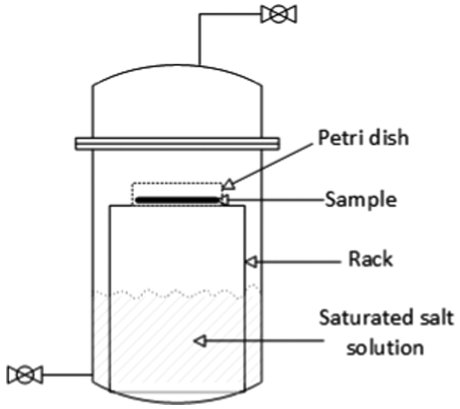

Figure 1. Polymeric film sample in humidity chamber with saturated salt solution for swelling test.

saturated solutions at room temperature. Here, the solutions are stated with equilibrium relative humidity at 25 °C in brackets: K_2SO_4 (97% RH), NaCl (75% RH), and $MgCl_2$ (33% RH). The water uptake of the membrane exposed to 33, 75, and 97% RH humidity in air, as explained and illustrated in Figure 1, was investigated.

The samples were removed from the chamber and weighed at regular intervals to determine the membrane water uptake from the gas phase in equilibrium with the saturated salt solution. After each weighing, the membrane was remounted into the chamber as quickly as possible and the lid of the chamber was kept loosely fit on the chamber during the weighing to minimize the disturbance to the system. This procedure was repeated until the film reached a constant weight (equilibrium water uptake). The water swelling degree (SD) of the membrane was calculated according to the following equation:

$$\mathrm{SD}\ (\%) = \frac{W_s - W_d}{W_d} \times 100 \tag{1}$$

where W_s and W_d are the masses of the swollen and dry membranes, respectively.

2.3. Contact Angle Measurement. A CAM 200 optical contact angle meter (KSV Instruments, Finland) with sessile drop method was used for the determination of the contact angle. A droplet of distilled water (3 μL) was carefully placed on the top surface of the membrane and the contact angles were determined using the high-speed optimum video analysis system. This unit is equipped with a FireWire camera module for measuring 100 images/s based on geniometry. A CAM 200 uses drop shape analysis for determining static contact angle, where the contact angle can be assessed by fitting the Young−Laplace equation to the drop profile. Using eq 2, each reported contact angle measurement is the average of 30 individual measurements.

$$\Delta P = (P_{\mathrm{int}} - P_{\mathrm{ext}}) = \gamma\left(\frac{1}{R1} + \frac{1}{R2}\right) \tag{2}$$

where ΔP is Laplace pressure, γ is surface tension, and $R1$ and $R2$ are the radii of curvature.

2.4. Surface Tension. The pendant drop method was used to determine the surface tension of the different PVAm membranes in solution (gas/liquid interface). The shape of the liquid drop hanging on the needle is determined from the balance forces, which include the surface tension of the liquid. The surface tension was determined by analyzing the drop shape of the following equation.

$$\gamma = \Delta\rho\, g \frac{R_0^2}{\beta} \tag{3}$$

where γ is surface tension, $\Delta\rho$ is density difference between fluids, g is gravitational constant, R_0 is radius of drop curvature at apex, and β is a shape factor that can be defined through the Young−Laplace equation expressed as three dimensionless first order equations (see SI for full details).

3. COMPUTATIONAL MODELS

3.1. Computational Details for Surface Properties. In this work, the computational protocols proposed in our previous work were applied for analyzing the wettability properties of the polymers and surface,[29] and gas transport properties through the membrane polymers based on molecular dynamics (MD) simulation.[30] All MD simulations were performed using (BIOVIA Materials Studio, v. 8.0, San Diego, 2017) commercial software. To obtain an accurate surface properties prediction at an atomistic scale, it is necessary to consider the force fields (FFs) employed, the cutoff for the nonbonded interactions, fractional free volume (FFV), density and conformation of the polymers, and FFs suitable for reproducing structural, thermodynamic, and dynamical properties of the polymer under conditions of thermodynamic equilibrium. The model of the polymer chain must be as accurate as possible. The condensed-phase optimized molecular potentials for atomistic simulation studies[31] (COMPASS) class II ab initio force field was used to describe the potential of the systems. COMPASS has been

DOI: 10.1021/acsomega.7b01307
ACS Omega 2017, 2, 8388−8400

Table 1. Physical Properties of PVAm[a]

system	energy	$e_{coh(sim)}$ (J/cm^3)	δ_{sim} (MPa$^{1/2}$)	ρ_{exp} (g/cm^3)	ρ_{sim} (g/cm^3)	NAC[b]	OV[c] (nm^3)	TVC[d] (nm^3)	FVC[e] (nm^3)	VF[f]	FFV[g] (cm^3/g)	SA[h] (nm^2)
pH 4	total	274	17	1.1	1.10	2720	13.96	19.97	6.01	30.10	0.091	132.61
	vdW	222	15									
	Q	54	7									
pH 10	total	1800	42	1	0.97	2480	13.6	22.76	9.00	65.41	0.214	152.11
	vdW	272	17									
	Q	1511	39									
pH 12	total	605	25	1.17	1.09	2420	13.3	19.81	6.28	31.70	0.112	142.62
	vdW	396	20									
	Q	197	14									

[a]Cell dimensions and simulated cohesive energy density (e_{coh}), solubility parameter (δ) and density (ρ) values at 298 K for PVAm and C-1,4PBD. [b]NAC: number of atoms per cell. [c]OV: occupied volume. [d]TVC: total volume of cell. [e]FVC: free volume of cell. [f]VF: void fraction. [g]FFV: fractional free volume. [h]SA: surface area.

demonstrated to be able to predict, with high accuracy, the densities of a number of liquids at different state points.[32,33] Moreover, the accuracy of COMPASS to treat polymers has already been demonstrated in other works[34] and has been extensively parameterized for gases, including He, H_2, O_2, N_2, and CO_2.[35] The COMPASS FF is the total potential energy of a molecular system, which in general terms is expressed as the sum of the following equations.

$$U_{pot} = U_{valence} + U_{cross\text{-}terms} + U_{nonbond} \quad (4)$$

$$U_{valence} = U_{bond} + U_{angle} + U_{torsion} + U_{oop} + U_{UB} \quad (5)$$

$$U_{cross\text{-}terms} = U_{bond\text{-}bond} + U_{angle\text{-}angle} + U_{bond\text{-}angle} + U_{end\text{-}bond\text{-}torsion} + U_{middle\text{-}bond\text{-}torsion} + U_{angle\text{-}torsion} + U_{angle\text{-}angle\text{-}torsion} \quad (6)$$

$$U_{nonbond} = U_{vdW} + U_{coulomb} + U_{H\text{-}bond} \quad (7)$$

The $U_{nonbond}$ interactions, which include a Lennard-Jones 9-6 function for the van der Waals (vdW) term and a coulomb function for electrostatic interactions, see eq 8, are used for interactions between pairs of atoms that are separated by two or more intervening atoms or those that belong to different molecules. The Lj-9-6 parameters (ε and r^0) are given for like atom pairs.

$$U_{nonbond} = \sum_{i,j} \varepsilon_{ij} \left[2\left(\frac{r_{ij}^0}{r_{ij}}\right)^9 - 3\left(\frac{r_{ij}^0}{r_{ij}}\right)^6 \right] + \sum_{i,j} \frac{q_i q_j}{r_{ij}} \quad (8)$$

The electrostatic interaction is represented using atomic partial charges, q_i, applied to each atomic species and derived from ab initio calculations. To make the charge parameters transferable, bond increments, δ_{ij}, which represent the charge separation between two valence-bonded atoms i and j, are used as parameters in the COMPASS FF. For atom i, the partial charge is the sum of all charge bond increments δ_{ij}.

$$q_i = \sum_j \delta_{ij} \quad (9)$$

where j represents all atoms that are valence-bonded to atom i.

3.2. Contact Angle Determination and Modeling Details. To achieve a good compromise between accuracy and computational time, the water model extended simple point charge model (SPC/E)[36] and 500 SPC/E water molecules were employed in the construction of the water droplet model.[37−40] The initial water cluster, corresponding to a cubic liquid water configuration with side length 2.46 nm and density ρ = 1 g/cm^3 (see SI for full details), was energetically optimized using the COMPASS FF.

This was done via a combination of conjugate gradient/Newton−Raphson iterations using a convergence criterion of 10^{-3} kcal/(mol Å), The particle mesh Ewald (PME) method[41] and an atom-based cutoff of 12.5 Å were used to treat electrostatic and Van der Waals interactions, respectively. This model is described in detail in our previous work.[29]

The generation of an accurate model of the amorphous polymer surface was conducted as follows: First, for the PVAm polymer, 6 chains with a degree of polymerization set to 12 were generated and subjected to energy relaxation using COMPASS. It is important to note here that although such small oligomers would hardly capture a genuine response to the behavior of a real polymer chain, it has been shown that all typical features of the fast segmental dynamics of interfacial polymer chains can indeed be explored using much shorter molecules.[42]

The conformational search was carried out using the combined molecular mechanics/molecular dynamics simulated annealing (MDSA) protocol.[43] According to this, the relaxed structure was subjected to five repeated temperature cycles (from 298 to 600 K and vice versa) using a canonical thermodynamic ensemble. In this protocol, the number of particles N, volume V, and temperature T, NVT, remain fixed in MD conditions. At the end of each annealing cycle, each structure was again energy minimized to converge below 10^{-4} kcal/(mol Å), and only those structures corresponding to the minimum energy were used for further modeling. The next step was to generate a cubic box starting with the optimized polymer chain and using the Theodorou and Suter version[44] of the rotational isomeric state method[45] at T = 298 K and applying the density of the polymer obtained from experiments. Table 1 displays these density values.

The model equilibration was conducted as follows: from the fully relaxed models of the corresponding polymeric chains, isothermal−isochoric (NVT) MD simulations were run at 298 K to equilibrate the systems and to ensure that their minimized total energy remains constant with respect to the timescale used in the simulation. To get the equilibrated bulk model polymer, the approach originally proposed by Rigby[34] was adopted. Thus, a cubic periodic cell of the polymer with a density close to the literature value at T = 298 K, after an initial energy

DOI: 10.1021/acsomega.7b01307
ACS Omega 2017, 2, 8388−8400

minimization, was subjected to 0.01 ns of *NVT* MD simulation using velocity scaling, to quickly establish the temperature, followed by 0.04 ns using the Andersen thermostat.[46] Density equilibration is then achieved by performing a further 1 ns of constant pressure constant temperature (*NPT*) MD simulations again using the Andersen thermostat and the Berendsen barostat.[47] The atom-based method with a cutoff of 9.5 Å was used to treat both electrostatic and van der Waals interactions.

To generate a large enough surface in the *XY* plane to prevent the droplet water molecules from interacting with each other in the periodic image, the periodic cells were replicated in x and y directions to yield final cell dimensions of PVAm as reported in Table 1. The modeling of individual components and the overall systems (i.e., water droplet on PVAm surface) was thus built. As a first step, to avoid interference of neighboring images in the vertical direction, the z dimension of the polymer cell was extended to 15 nm. Then, the equilibrated water droplet was placed and centered on the top of the polymeric surface at an initial distance of about 3 Å. The resulting system was relaxed and subsequently subjected to 1250 ps of *NVT* MD simulations at T = 298 K, keeping the polymeric surface fixed. The Ewald method[41,48] was applied for treating all nonbonded interactions. The Berendsen thermostat with a decay constant of 0.1 ps, as discussed in Manias and Kuppa,[42] was adadopted for temperature control, and 1 fs was chosen as the Verlet integration time step. The first 750 ps of the MD simulation was required to reach the equilibrium state, monitored by the large and rapid decay of the average internal energy of the system followed by a steady plateau. The remaining 500 ps of equilibrated MD trajectory was used for data harvesting and analysis. To determine the contact angle (CA), the computational protocols proposed in our previous work[29] were employed, in which the θ value of a spherical liquid droplet on a given (e.g., polymeric) surface was obtained from the relevant equilibrated MD trajectories.

3.3. Contact Angle Analysis. The relationship between contraction force (surface tension) and attraction force (surface free energy) was integrated in the contact angle measurement. There are two different modes of contact angle: (1) static or equilibrium CA is when the water droplet reaches equilibrium and thus will not change over time, and (2) dynamic or hysteresis CA is when the water droplet will change continuously as a function of time. The dynamic wetting (contact angle), liquid penetration (volume), and spreading are all measured as a function of time.

The strength of the attractive or repellent force is closely related to the contact angle between the water droplet and the surface. Characterizing the water contact angle on a PVAm surface is very challenging due to its hydrophilicity and water absorption potential. Macroscopic determination of hysteresis contact angle was therefore performed in the wettability analysis: The experimentally obtained contact angle of a drop placed on a PVAm surface has a value ranging between the so-called advancing (maximum) at the three-phase contact advancing angle, θ_A, to the so-called receding (minimum) contact angle, θ_R at the contact line. When the receding angle is subtracted from the advancing angle, the result is called the contact angle hysteresis, $\theta_A - \theta_R = \Delta\theta_{hyst}$. The Young equilibrium contact angle is somewhere between those values, however, the microscopic behavior of contact angle from the MD simulations may well represent the equilibrium contact angle, hence the measurement-determined $\Delta\theta_{hyst}$ is expected to be comparable with $\theta_{Sim.}$

3.4. Attraction Forces. A traditional way to interpret the forces of the liquid–solid interface is to apply Young's law as a force balance of surface tensions. However, to properly reach the equilibrium of the forces,[49−51] it has been demonstrated in the literature that the complete interpretation of three forces exerted on the system is needed. (Consult the SI for further discussion on this force balance.) Two forces are added: attractive force $\gamma_{liq} \sin\theta$, which is called the reaction of the surface R_s, and the net repulsive force $Net_{RF} = \gamma_{pol} - \gamma_{int}$, which also acts in the contact line.

For a better understanding of the wetting behavior of the PVAm surfaces, the microscopic interpretations of wetting were taken into consideration. This can be modeled as two parallel forces acting in the contact line[52] liquid on solid $\gamma_{liq}(1 + \cos\theta)$ and solid on liquid $\gamma_{liq} \sin\theta$ (see SI for full details).

3.4.1. Liquid on Solid—Work of Adhesion (W_{adh}). The contact angle θ values obtained for polymer–water systems were then used to obtain the corresponding values of work of adhesion by means of the Young–Dupré equation,[53] see eq 10.

$$W_{adh} = \gamma_{liq}(1 + \cos\theta) \tag{10}$$

where γ_{liq} = 73 (mJ/m^2) is the surface tension of water from the literature.[54]

3.4.2. Solid on Liquid—The Net Normal Force. The main reason for the existence of this force is the unbalanced forces in the solid–liquid outside the droplet interface (see SI for full details). It originates from the differences of the repulsive forces inside $\gamma_{pol} + \gamma_{liq} - \gamma_{int}$ and outside $Net_{RF} = \gamma_{pol} - \gamma_{int}$ of the droplet, the unbalance of these forces is equal to $\gamma_{LV} \sin\theta$. This resulting net normal force of the unbalance is called the reaction of the surface (R_s).[52]

3.5. Repulsive Forces. *3.5.1. Liquid–Solid Interface Surface Tension (γ_{int}).* The Duprè equation was used to calculate γ_{int}, as shown in eqs 11 and 12. The solid–liquid surface tension represents the free energy needed to create a solid–liquid interface. According to eq 2, the attraction of the solid–liquid interface reduces the surface energy due to W_{adh}.

$$W_{adh} = \gamma_{pol} + \gamma_{liq} - \gamma_{int} \tag{11}$$

$$\gamma_{int} = \gamma_{pol} + \gamma_{liq} - W_{adh} \tag{12}$$

where W_{adh} is work adhesion, γ_{liq} is surface tension of the liquid, γ_{pol} is surface tension of the surface polymer, and γ_{int} is the interfacial tension between them.

3.5.2. Net Repulsive Force. The repulsive force $\gamma_{pol} + \gamma_{liq} - \gamma_{int}$ is continuous along the surface and zero outside the droplet (see SI for full details). To calculate the net repulsive force between the subsystems, the attractive force γ_{liq} was subtracted from the repulsive force $\gamma_{pol} + \gamma_{liq} - \gamma_{int}$ yielding

$$Net_{RF} = \gamma_{pol} - \gamma_{int} \tag{13}$$

4. RESULTS AND DISCUSSION

The degree of hydrophilicity manipulation of a given surface requires understanding the microscale principles that, in turn, control the macroscale surface-wetting behavior. Hence, understanding the structure and performance of a common fluid such as water at the interface with PVAm is of great and practical importance when, for instance, this polymer is being used for separation of gas components present in a humid flue gas.

DOI: 10.1021/acsomega.7b01307
ACS Omega 2017, 2, 8388−8400

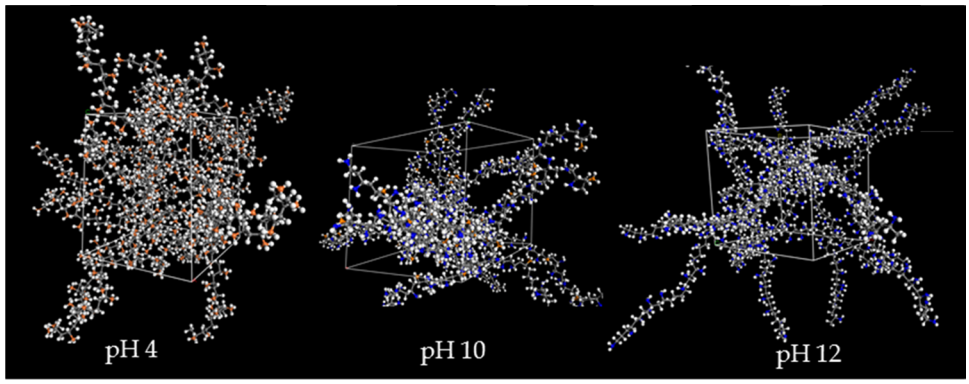

Figure 2. Snapshots of the chains conformation of PVAm equilibrated from MD simulations at pHs 4, 10 and 12. Orange atoms correspond to the amine protonation.

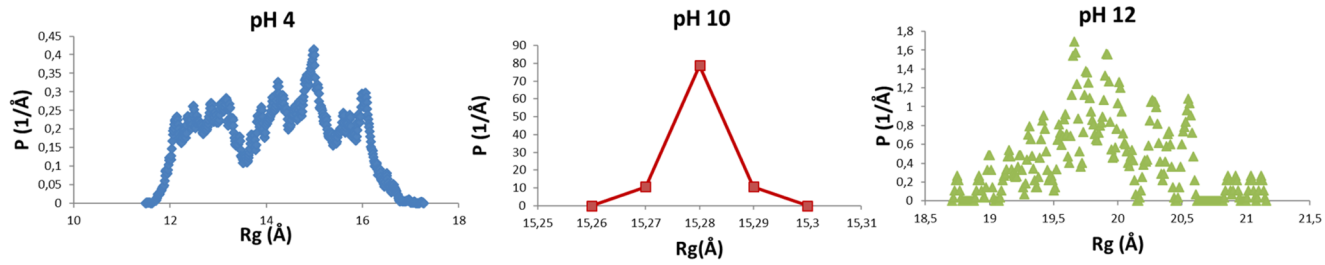

Figure 3. Probability of polymeric chain distribution in function of radii of gyration—R_g.

4.1. Physical Properties. Intramolecular interaction of PVAm at different pH values was studied by cohesive energy density (e_{coh}), solubility parameter (δ), and the chain packing density with the fractional free volume (FFV). As is well known, thermophysical and mechanical properties are directly related to the cohesive energy, and therefore they become the first step of study.

Atomistic simulations were conducted to calculate intramolecular forces within solid (PVAm) and liquid (water) interfaces: polar interactions (van der Waals), ion−ion (+ −), ion−dipole (H-bond), dipole−dipole, dipole-induced dipole, and a-polar interactions (hydrophobic dispersion, coulomb forces (Q)). The background theory for these simulations is explained in paragraph 3.

The physical properties of PVAm are given in Table 1. The fully protonated form of PVAm at pH 4 shows the lowest dispersive (vdW) and electrostatic (Q) intramolecular interactions, whilst the unprotonated form of PVAm at pH 12 yields an almost two times increase in the vdW and Q interactions. In the intermediate state, PVAm at pH 10 presents the largest interactions, and hence highest values of e_{coh}, δ, and FFV. Figure 2 shows the pH response of different conformations of PVAm: the entangled polymer chains at pH 4 are very tight and contracted due to the high electrostatic repulsion of the H-bonding. Hence, at this pH, it is a more fragile and more brittle polymer. In the case of pH 12, the repulsions are low, yielding increased mobility and FFV. This leads to an increased amorphous polymer structure. At the intermediate condition, pH 10, the polymer chains are less entangled due to the balance between the electrostatic forces and dispersion forces (ion−dipole, H-bond). This consequently generates free space between the chains. The repulsive interaction between PVAm protonated (pH = 4) and unprotonated (pH = 12) thus turned out to be largely influenced by steric hindrance of the protonated amine group.[55]

This behavior of pH 10 PVAm could be explained due to the orientation and the conformation packing density of the chain polymer, which allows a very high strength of attractive and repulsive forces to form between the protonated and unprotonated amine groups. There is a balance of intermolecular forces at this pH that allows the strength and stability of the polymer chain to increase. The steric hindrance, force balance, and hydrogen bonding are the key factors for the PVAm microgel formation and therefore the main factors for polymer stability.

Because of the polyelectrolyte effect, as is well known, PVAm is a highly cationic polyelectrolyte, which means that the oppositely charged polymer sites attract one another and bind together. The intramolecular interactions such as the cohesive energy density and solubility parameters of PVAm are not linearly dependent on pH. However, the hydrogen bonding is strongly dependent on the protonation state of the amine group.[55] The intramolecular interactions of PVAm are strongly influenced by the steric hindrance of the amine protonation and the chain packing density caused by the attraction and repulsion force balance of the protonated and unprotonated neighboring amine groups.

To gain more information on the conformation of the polymer chains, the diameter sizes were quantified by considering the values of the radius of gyration of the polymer structure; where the radius of gyration R_g is defined as the root mean square (RMS) distance of the collection of atoms from their common center of gravity. Radius of gyration of a polymer coil was calculated using the following equation.

$$R_g = \sqrt{\sum \left(\frac{x_i^2 + y_i^2 + z_i^2}{N} \right)} \tag{14}$$

where N is the number of atoms and x, y, and z are the atomic coordinates relative to the center of mass.

DOI: 10.1021/acsomega.7b01307
ACS Omega 2017, 2, 8388−8400

It can thus be concluded that the greater stability of PVAm at pH 10 is due to the morphology blend of the partial amorphous region and partial crystalline region, moreover, also to the steric hindrance caused by the protonated state of PVAm and the chain packing density caused by the attraction and repulsion force balance among the protonated and unprotonated neighboring amine groups. These reasons play a critical role in the morphology of the polymeric structure and consequently in the stability and wetting behavior of PVAm.

Figure 4 shows X-ray diffraction patterns obtained by molecular dynamic simulations. The measurable scattering reflects the pattern of interference between the scatterings from all of the atomic centers. At pH 10, the crystallinity zones with very intensive diffraction peaks are arranged in a periodic array, and the amorphous zone has a wide range curve. At pH 12, no distinct diffraction peak can be detected, and the polymer conformation is judged as amorphous. pH 4 shows a diffraction peak and narrow curve, thus indicating crystalline and amorphous zones.

Figure 3 shows the probability of polymeric chain distribution as a function of the radius of gyration R_g based on molecular dynamic simulations. For PVAm at pH 4, it is in the range of 11−17 Å with a very broad probability distribution. This indicates that the polymeric chain has a wide range of polymeric conformations. In the case of pH 10, a sharp localized peak is found with very high probability at 15 Å, suggesting that there is one preferred polymer chain conformation and therefore a more stable system. This could be due to the steric hindrance for the partial amine protonated sites, which has a high impact on the morphology of the PVAm chain and potentially increases the degree of crystallinity. At pH 12, there is again a broad probability distribution with different chain conformations from 18.7 to 21 Å. This indicates a high degree of amorphous region and low degree of crystallinity.

4.2. Surface Properties. Intermolecular interactions of PVAm at different pHs were studied by contact angle θ, attraction forces (surface tension γ_{liq} and γ_{pol}, work adhesion W_{adh}, and reaction from the surface R_s) and repulsion forces (interface surface tension γ_{int} and net repulsive force). PVAm exhibited three-stage wettability switching from pH 4 (fully protonated), pH 10 (partial protonated), and pH 12 (unprotonated) (Figure 4).

4.2.1. Fully Protonated PVAm Wettability. As seen in Figure 5a, the macroscopic behavior of water contact angle on the PVAm surface at pH 4 shows high adsorption in a short time span, where the experimental contact angle (CA) goes from $\theta_A = 70°$ to $\theta_R = 0°$ in 5 s. Therefore, there is no $\Delta\theta_{hyst}$ or swelling behavior at pH 4. It is also evident from Figure 5d that the baseline remains constant over the time, which means that the surface of the water droplet is not changing. This indicates that there is no water spread on the polymeric surface, i.e., the water molecules are holding together. The drop volume decreasing over the time, as seen in Figure 5g, means the attraction forces as shown in Table 2 (W_{adh} = 106 mJ/m^2 and R_s = 65 mJ/m^2) are weaker than the repulsive forces (γ_{int} = 37 mJ/m^2 and Net_{RF} = 33 mJ/m^2) at low pH. When the liquid is on the solid, the adhesion is low (W_{adh} = 106 mJ/m^2), and the main interaction is the unbalanced force in the solid−liquid outside the droplet interface, where the reaction of the surface at R_s = 65 mJ/m^2 is very high. This can be explained because the water molecules are attracted by the charge density of the surface and can be absorbed easily on the surface.

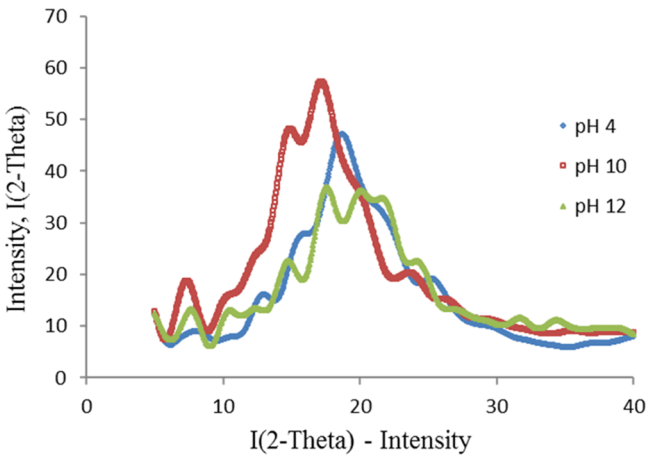

Figure 4. X-ray diffraction structure from MD simulations.

The PVAm adsorption at low pH 4 is electrostatically driven and forms very thin adsorbed layers. The main reason for the PVAm−water adsorption at low pH 4 is due to the excess positive charge of the polymer at this pH; hence, this causes a strong electrostatic interaction with the negatively charged end of water (the oxygen atom). There are weaker equilibrium forces, and the polymeric protonated state at pH 4 provides a very high interfacial surface energy, γ_{int} = 37 mJ/m^2. In this way, the high water adsorption at low pH is due to excessive repulsive charge on the surface and the high inter/intramolecular H-bonding between fully protonated groups.

The surface tension of PVAm at low pH (see Table 2, γ_{pol} = 70 mJ/m^2) is close to the surface tension of water (γ_{liq} = 73 mJ/m^2), and therefore the surface cannot break the surface tension of the liquid and spread the water molecules. This can be observed more clearly at a microscopic level in the equilibrium contact angle from the MD simulations, as shown in Figure 6.

4.2.2. Partial Protonation of PVAm Wettability. In the case of wettability, partial protonated PVAm shows a higher resistance and therefore a decrease in hydrophilic behavior, as seen in Figure 5b. For the macroscopic level contact angle of PVAm at pH 10, it shows high stability. The contact angle stays constant during the first 40 s, and then drops to 67° as the swelling of the surface starts from 40 to 100 s, before returning to 120°. The surface is showing contact angle hysteresis, with an advancing angle $\theta_A = 112°$, retracting angle $\theta_R = 67°$, and yielding $\Delta\theta_{hyst} = 45°$. The partial protonated surface of PVAm shows a high stability even in the swollen state.

In Figure 5e, the baseline increases with time from 40 s, which means that the water droplet spreads on the surface after 40 s, and the surface tension of water molecules was overcome by the surface energy of PVAm (the droplet volume in Figure 5h, the first contact shows stability, no water absorption up to 40 s). Then, water starts absorbing and at the same time swelling the surface until 100 s. Table 2 shows the behavior of water absorption on the PVAm surface, the high stability could be explained by the balance of attraction forces γ_{pol} = 62 mJ/m^2, W_{adh} = 122 mJ/m^2, and R_s = 54 mJ/m^2 and repulsive forces γ_{int} = 22 mJ/m^2 and Net_{RF} = 40 mJ/m^2. Water is less attracted by the charge density of the surface, even though there is adsorption of water molecules on the surface. The equilibrium and the stability in the contact line give the potential of swelling the polymer without damaging the polymeric chain conformation. This indicates that the high inter/intramolecular H-

DOI: 10.1021/acsomega.7b01307
ACS Omega 2017, 2, 8388−8400

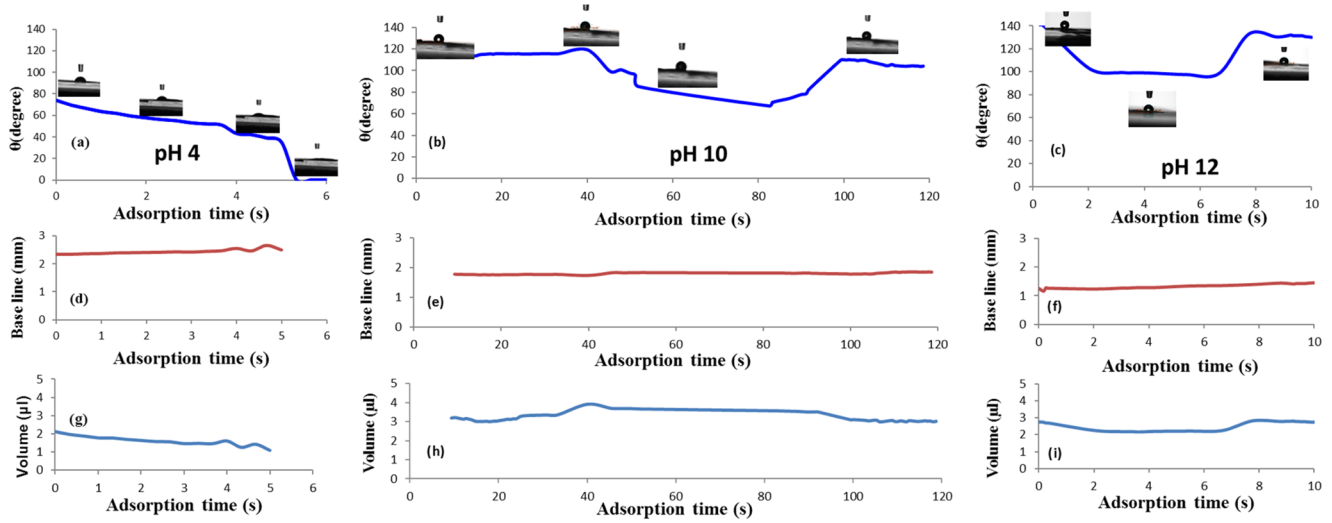

Figure 5. (a–c) Adsorption time of water on PVAm surface at pHs 4, 10, and 12. (d–f) Baseline of three-phase contact radius and (g–i) drop volume as a function of time.

Table 2. Contact Angle θ (deg), Surface Tension γ (mJ/m^2), and Work of Adhesion W_{adh} (mJ/m^2) for Water in Contact with a PVAm Surface at Different pHs[a]

	contact angle				attraction forces			repulsive forces	
	exp			sim					
system	θ_A (deg)	θ_R (deg)	$\Delta\theta_{hyst}$ (deg)	θ_{equi} (deg)	γ_{pol} (mJ/m^2)	W_{adh} (mJ/m^2)	R_s (mJ/m^2)	γ_{int} (mJ/m^2)	Net_{RF} (mJ/m^2)
pH 4	70			63(62)[b]	70(72, 73)[c]	106	65	37	33
pH 10	112	67	45	48	62	122	54	22	40
pH 12	140	98	42	41	60	128	48	5	55

[a]Available experimental values from the literature are shown in parentheses for comparison. [b]Ref 56. [c]Refs 57, 58.

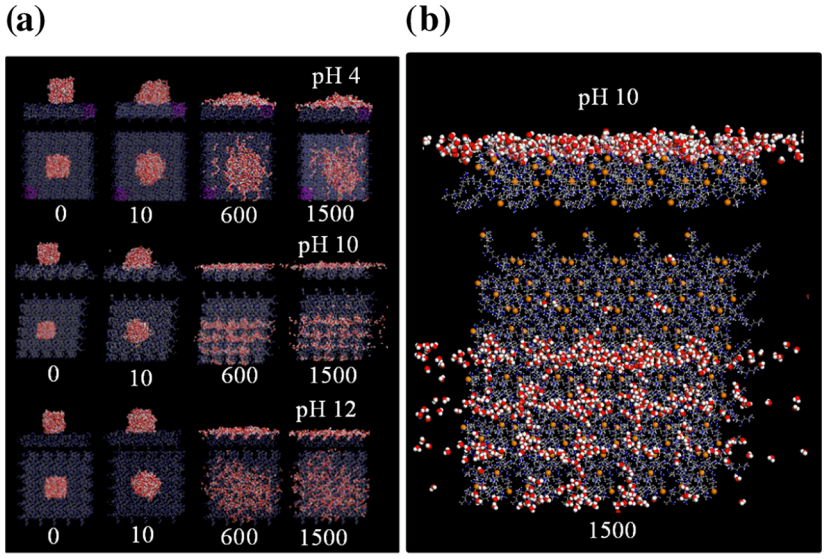

Figure 6. (a) Left side, snapshots (top and side views) of the dynamics course of water spreading on the PVAm surface at pHs 4, 10, and 12. (b) Right side, detailed view of PVAm at pH 10, orange atoms correspond to the conformation of amine protonation.

bonding between protonated and unprotonated amine groups plays a critical role in the wettability of the PVAm surface.

The partial protonated form of PVAm at pH 10 provides a low interface surface energy, γ_{int} = 22 mJ/m^2. Hence, lower water adsorption at high pH is due to the balance of attractive forces and repulsive charge on the surface. The surface tension of the polymer is lower, γ_{pol} = 62 mJ/m^2, than that of water, γ_{liq} = 73 mJ/m^2, see Table 2, and the PVAm surface can break the water surface tension, and therefore it can spread the water molecules on the surface due to the partial charge density at pH 10.

This behavior can also be seen in Figure 6 in the pictures of the dynamics of PVAm at pH 10, showing how water is spreading on the PVAm surface in a detailed view (top and side view). The distribution of the water molecules and the charge density of the polymer chain stick together, forming patterns as

DOI: 10.1021/acsomega.7b01307
ACS Omega 2017, 2, 8388–8400

holes in structures on the surface. However, where the surface has no charge, water can easily penetrate the chains of polymer and fill the free volume and swell the polymer.

Water can penetrate the polymer and untangle the polymer chains due to the holding physical forces, and transform them from a static solid state to a more viscous liquid state. The electrostatic interaction is predominant, causing full dissociation of amine groups. The H-bonding between protonated and unprotonated amine groups, the conformation polymer chain, and the distribution charge density all play a crucial role in the surface stability and wettability properties.

4.2.3. Unprotonated PVAm Wettability. The wettability of unprotonated PVAm decreases the hydrophilic behavior, as can be seen in Figure 5c where the macroscopic level contact angle of PVAm at pH 12 shows a lower stability up to 10 s. The hysteresis contact angle of unprotonated PVAm at pH 12 varies from $\theta_A = 140°$ down to $\theta_R = 98°$, thus $\Delta\theta_{hyst} = 42°$. In Figure 5f, the baseline increases as a function of time, meaning that the water droplet is spreading on the surface within 10 s. The drop volume in Figure 5i decreases, indicating that the water absorption is fast, and starts to swell the polymer.

Table 2 shows the attraction forces $\gamma_{pol} = 60$ mJ/m^2, $W_{adh} = 128$ mJ/m^2, and $R_s = 48$ mJ/m^2 and repulsive forces $\gamma_{int} = 5$ mJ/m^2 and $Net_{RF} = 55$ mJ/m^2. These forces are not in equilibrium, because the attraction forces are higher at lower pH. This is due to the low interface surface energy $\gamma_{int} = 5$ mJ/m^2 and very low intermolecular interaction on the contact line. In this case, PVAm is probably capable of interacting with water molecules through hydrogen bonding, and at these conditions, this promotes water spread. For PVAm at high pH, there are no electrostatic interactions; the attraction contribution is from the dispersive vdW interactions. Figure 6 shows snapshots of the dynamic simulations, a remarkable homogeneity of the water molecules on the PVAm forms a flat surface of water molecules.

Up to this point, the horizontal attraction, W_{adh}, forces have been considered, however as discussed, W_{adh} forces are functions of the charge density of the protonation of the amine groups. For high charge density and low W_{adh}, it is, however, important to consider the vertical attraction, as the reaction surface, R_s, goes down. At high charge density and high R_s, the attraction and repulsion forces of PVAm at pH 10 are in equilibrium and hence more stable.

As can be seen in Figure 7, another factor, which helps to analyze the stability of PVAm at different pH, is the time needed to identify the contact angle equilibrium by molecular dynamic simulations. The equilibrium for the contact angle at pH 4 and pH 12 takes longer, around 1100 ps to reach equilibrium, whereas in the case of pH 10, it reaches equilibrium faster after ca. 650 ps and remains constant.

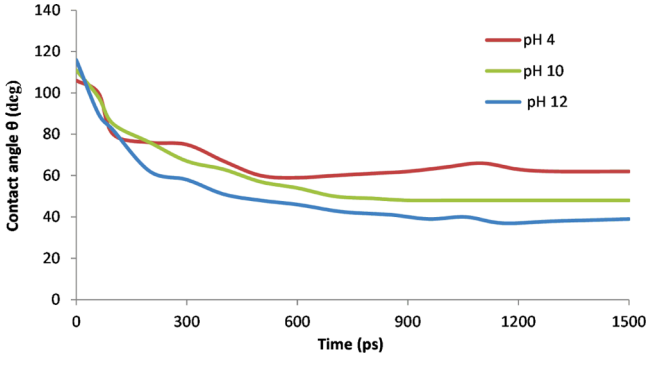

Figure 7. Contact angle vs time of PVAm at different pH values of 4,10, and 12 by molecular dynamic simulations.

4.3. Structural Analysis—RDFs. As already discussed, the formation of hydrogen bonds plays an important role in the wettability properties of water on the PVAm surface. To quantify intermolecular interactions and their contribution to the structural properties of water, analysis of the radial distribution function (RDF) is helpful to understand the microscopic behavior of molecules for these interface systems. A series of RDFs are shown in Figure 8. The appearance of peaks in the radial distribution function is due to intermolecular collisions or the repulsive forces arising inside.

Attractive forces are responsible for a significant high density. Moreover, as can be seen in the case of water, the existence of strong and directional attractive forces (such as hydrogen bonding) can significantly modify the structure of the peaks.

Figure 8a shows the fully protonated amine (pH 4), where the attraction forces between $g_{N(amine)-O(water)}(r)$ and hydrogen bonding between amine−water have equal contributions in the intermolecular interaction at short range. However, at long range, the dispersive forces increase significantly. Figure 9 shows that the H(water)-bond acts as a donor and the H(amine)-bond acts as an acceptor.

In the case of partial protonation, PVAm has three options for hydrogen bonding, two from the protonated state and one from the unprotonated state. In Figure 8b the very large peak at 3 Å is due to the hydrogen bond between $g_{H(amine)-O(water)}(r)$, corresponding to the unprotonated state, where the H(water)-bond acts as electron acceptor and the H(amine)-bond acts as electron donor. The high interaction density of this hydrogen bond and the high intensity of interaction are the main contributions to the stability of PVAm at pH 10.

The second peak at 3 Å at low intensity corresponds to the attraction between $g_{N(amine)-O(water)}(r)$, whereas the third peak at 3.20 Å corresponds to the second hydrogen bond from the unprotonated state $g_{N(amine)-H(water)}(r)$. In this unprotonated case, the H(water)-bond acts as electron donor and the H(amine)-bond acts as electron acceptor, see Figure 9.

The small peak at 3.5 Å corresponds to the third hydrogen bond in the protonated state, likely in the crystalline region of the linear polymer chains, which are structurally oriented in a uniform three-dimensional matrix, $g_{N(amine+)-H(water)}(r)$. This shows very low interaction at short range (Q) but very high contribution in the long range (vdW). This is due to the H(water)-bond acting as an electron donor and N(amine)-bond acting as electron acceptor.

The high stability of PVAm at pH 10 occurs because the hydrogen bond becomes collectively stronger due to the many molecules bounded, and the great solubility corresponds to the hydrogen bond between $g_{H(amine)-O(water)}(r)$ from the unprotonated state and to the overall stiffness of the structure. The interchain hydrogen bonding between the amine−water could also enhance the stiffness. The PVAm molecules align themselves side by side into hydrocarbons that are stabilized by interchain hydrogen bonding with water.

Moreover, the $g_{H(water)-N(amine+)}$ bond likely acts as a physical crosslink through the interchain polymer conformation at the protonation state, see Figure 10; this H-bonding $g_{H(water)-N(amine+)}$ enhances the crystallinity and increases dramatically the inter-laminar space of the crystalline zone, thus reducing the interchain free space and increasing the interaction between amorphous and crystalline interchains.

DOI: 10.1021/acsomega.7b01307
ACS Omega 2017, 2, 8388−8400

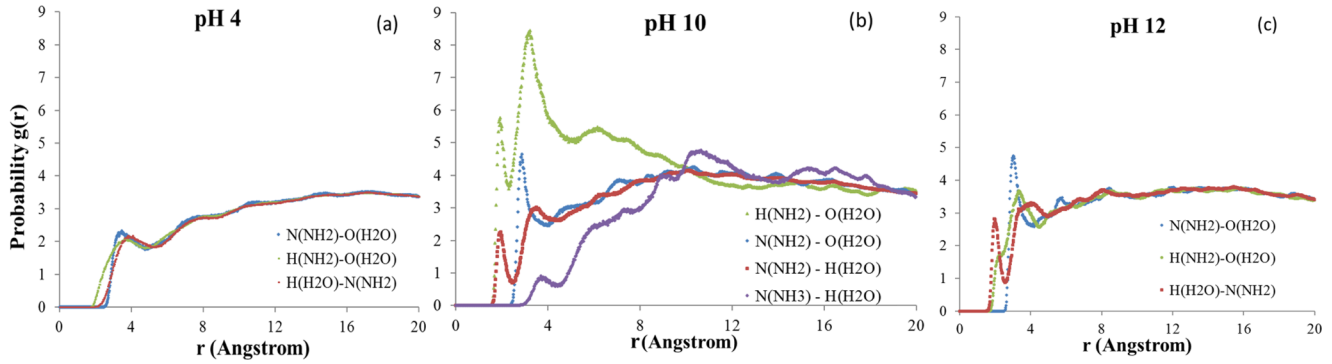

Figure 8. RDFs of (a) pairwise N(amine), H(amine) O(water), and H(water), (b) N(amine), H(amine) O(water), H(water), and N(amine$^+$), and (c) pairwise of N(amine), H(amine) O(water), and H(water).

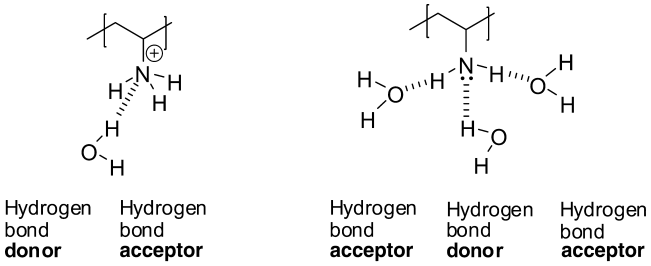

Figure 9. Hydrogen bond acceptor and donor from amine protonated and unprotonated with water.

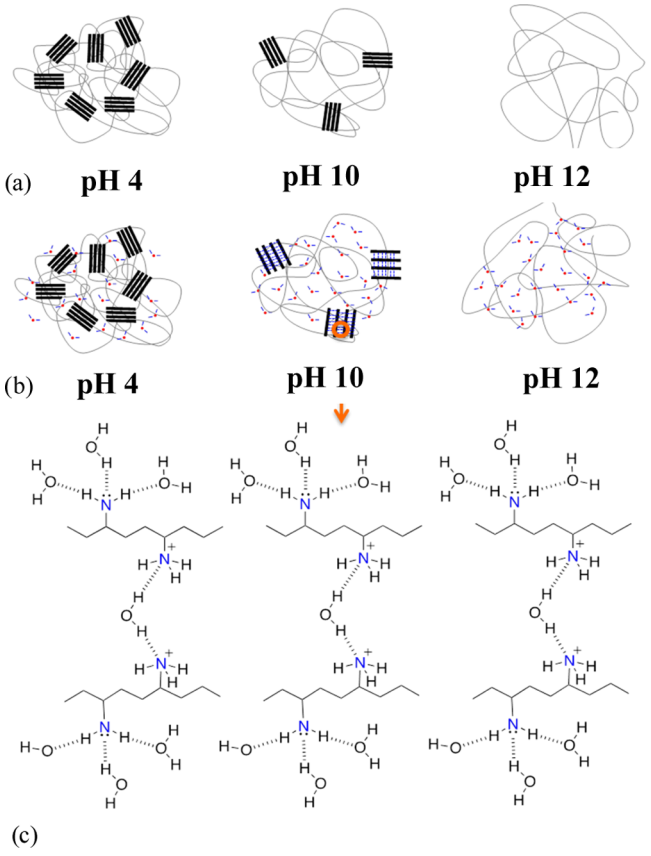

Figure 10. (a) Sketch of crystalline and amorphous polymer states at different pHs, (b) sketch of inter/intramolecules of crystalline and amorphous PVAm with water molecules, and (c) hydrogen bond between water−amine protonated acts as physical crosslink.

This makes the polymer more mechanically resistant and therefore more stable; moreover, the strong inter/intramolecular forces in the short (electrostatic forces) and large range (dispersion forces) also play an important role in the interactions.

The unprotonated state of PVAm in Figure 8c shows less interaction with water molecules. Both hydrogen bonds are in the same low range of interaction, the peak at 3 Å corresponds to the attraction between $g_{N(amine)-O(water)}(r)$, the second peak at 3 Å corresponds to the $g_{H(amine)-O(water)}(r)$, wherein the H(water)-bond acts as acceptor and the H(amine)-bond acts as donor. The third peak at 2.2 Å corresponds to the second hydrogen bonding $g_{N(amine)-H(water)}(r)$, but in this case, the H(water)-bond acts as donor and the H(amine)-bond acts as acceptor.

4.4. Binding Energies. To analyze the intermolecular interactions between PVAm/water, binding energy simulations were performed by molecular dynamic simulations in the canonical (NVT) ensemble and were run at T = 298 K. From the equilibrated part of the MD trajectory of each PVAm system, the interaction energies among all system components were extracted according to a well-validated procedure.[59] Because, by definition, the binding energy (E_{bind}) between each generic pair of PVAm system components (PVAm) and water is the negative of the corresponding interaction energy, each E_{bind} term can simply be obtained from the corresponding interaction energies as shown in eq 15[59]

$$E_{bind\ (PVAm/water)} = E_{PVAm} + E_{water} - E_{PVAm}/E_{water} \quad (15)$$

Interaction energy terms between the polymer and water, $E_{bind(PVAm/H_2O)}$, increase when protonation decreases. Generally, water molecules preferably interact more when the amine is unprotonated, by virtue of strong Coulombic attraction between the water dipoles and amine group. The more protonated form of the PVAm surface possesses the potential to realize larger segment/PVAm surface contacts, which favors surface adsorption and, ultimately, results in the highest level of polymer interaction with water.

As can be seen in Table 3, pH 4 presents the lowest interaction; the Coulombic forces are predominant due to the charge density of PVAm. The conformation of the protonated polymer and the rigidity of the chain polymer reduce the interaction space between amine groups and water.

For pH 10 and pH 12, the potential energies are almost three times higher due to the free space formed in untangled polymer conformation. However, pH 10 presents the highest interaction energy, due to the high FFV of the chain polymer conformation

DOI: 10.1021/acsomega.7b01307
ACS Omega 2017, 2, 8388−8400

Table 3. Binding Energies from Water on PVAm ($E_{bind(PVAm/H_2O)}$) at Different pHs: 4,10, and 12[a]

energy	pH 4	pH 10	pH 12
potential	−994	−2615	−2323
vdW	−215	−78	−150
coulomb	−779	−2537	−2173

[a]All energies are in kcal/mol.

and the mobility of the unprotonated amine groups. Thermodynamic arguments can be invoked to account for this trend. Indeed, it can be argued that PVAm would generally adopt a conformation that allows for maximum segment-surface interactions.

H-bonding between $g_{H(water)-N(amine+)}(r)$ acts as a physical crosslinker between the polymer chains, giving greater rigidity and strength to the polymer matrix.

4.5. Swelling Properties. Figure 11 shows the swelling kinetics of PVAm samples a, b, and c at room temperature, over different saturated salt solutions (yielding a defined and constant relativity humidity RH%). Figure 11d–f shows the samples with different pHs. Generally, the swelling degree (SD %) behavior increases when the RH% increases; this effect is governed by the effect of intra-chain hydrogen bonding on crystallinity zone of PVAm. At pH 4, there is full protonation (high content of crystalline zone), and at pH 10 and partial protonation (crystalline and amorphous zones), there is a high capacity for swelling the polymer chain, whereas at pH 12, there is the lowest capacity. Another interesting point of the swelling kinetics is the time to reach the equilibrium. At pH 4 and 12, it takes about 100 h before the equilibrium at different RH% is reached.

However, at pH 10, a plateau is reached after about 100 h followed by a slow almost linear increase before reaching the equilibrium at 850 h. This reflects the greater stability of the polymer due to the effect of intra-chain hydrogen bonding on the crystallinity zone of PVAm and the physical crosslinked effect of H-bond (water) and given amine protonation.

The 37% swelling degree at pH 10 reflects the ability of the polar groups to interact with water molecules in this conformation of the polymer matrix. This is due to the physicochemical affinity of the polymer group to water, the free space available in the vicinity of the sites, as well as the local elastic resistance of the chains to swelling deformation stress.[60]

Water penetration is different in the three pH levels of PVAm measured, and it depends on the hydrogen bond formation. The PVAm conformation is pH driven, from amorphous to crystalline state.

At pH 4, the polymer matrix presents more crystalline regions that cannot arrange themselves as freely as those of pH 10 and 12, which present more amorphous regions. The principal factor affecting the crystallization is the polarity of the molecules, which increases the attraction between adjacent chains, and hence induces the crystallization.

As seen in Figure 12, PVAm surface properties are a function of the protonation state; at high protonation degree: much

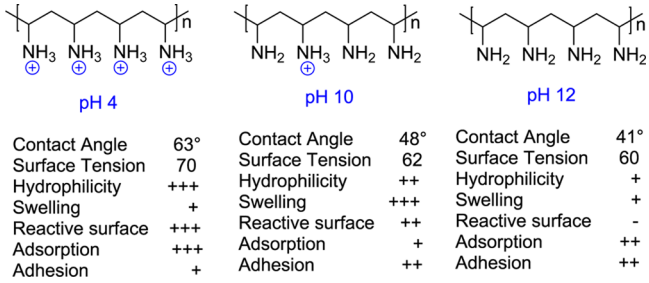

Figure 12. Schematic illustration of the chemical structure and surface properties of PVAm at different protonation: contact angle "CA" (deg), surface tension "ST" (mJ/m^2), hydrophilicity "HF", and swollen "SW" for water in contact with a PVAm surface at different pHs.

hydrogen bonding and large vdW forces are increasing the intramolecular interactions between PVAm and water. The wettability behavior of the PVAm surface is hence also a function of pH.

5. CONCLUSIONS

In the current work, the wettability properties of PVAm cast from solutions of different pHs have been documented, both by

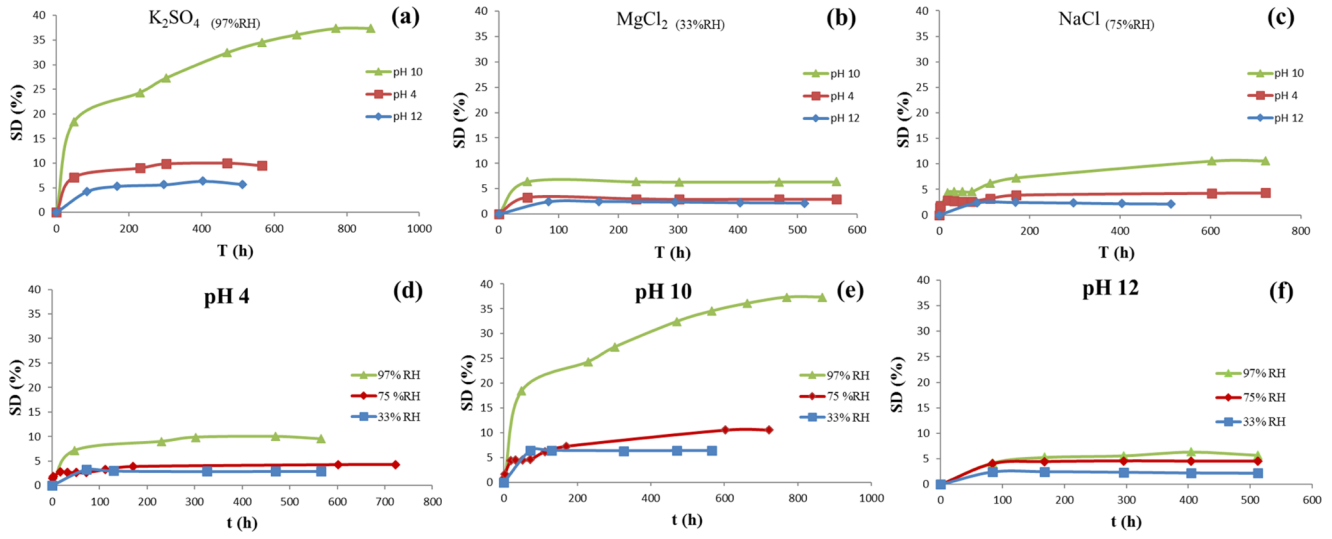

Figure 11. Swelling kinetics of PVAm samples a, b, and c at room temperature in different salt solutions (relativity humidity RH%). d, e, and f samples with different pHs.

DOI: 10.1021/acsomega.7b01307
ACS Omega 2017, 2, 8388−8400

experimental and molecular dynamic simulations, confirming that the intramolecular interactions such as the cohesive energy density (echo) and solubility parameters of PVAm are pH-dependent.

It was found that the high stability of pH 10 polymer is due to the orientation and the conformation of the packing density of the polymer chain, which allow a very high strength of attractive and repulsion forces to be formed between the protonated and unprotonated amine groups. There exists a balance of intermolecular forces that allows the strength and stability of the polymer chains to be increased. The steric hindrance, force balance, and hydrogen bonding are all key factors with respect to the PVAm microgel formation, and therefore, they are the main factors for polymer stability. This work confirms by structural analysis of RDFs that the high stability of PVAm at pH 10 is because the hydrogen bond becomes very strong because many molecules are bound, inducing stiffness to the overall polymeric matrix. The high water solubility corresponds to the hydrogen bond between $g_{H(amine)-O(water)}(r)$ from the unprotonated state.

The intramolecular interactions of PVAm (for any investigated pH) are strongly influenced by the steric hindrance of the amine protonation and the chain packing density caused by the attraction and repulsion force balance of the protonated and unprotonated neighboring amine groups.

The high inter/intramolecular H-bonding between protonated and unprotonated amine groups, the conformation polymer chain, and the distribution charge density play a crucial role in the surface stability and wettability properties.

PVAm in a charged state is not surface active, as it reduces the mobility of the amine groups. When the surface is unprotonated, it is more surface active, experiencing more mobility of the amine groups. In the case of the partial charge state, both features combine giving enough strength and mobility to swell the polymer and the capability of being more stable.

This work confirms that PVAm is pH dependent of the surface tension, reflecting the dissociation behavior of the amine group exploiting the concomitant swelling (charged state) and partial collapse (neutral state). PVAm at pH 4 and 12 shows the typical behavior of a linear polymer, whereas at pH 10, it behaves as a microgel. A balance occurring at pH 10 of PVAm between the attraction and repulsion forces of water on PVAm surfaces helps to maintain the stability of the membrane for CO_2 transport.

Moreover, the $g_{H(water)-N(amine+)}$ bond likely acts as a physical crosslinker through the interchain polymer conformation in the protonated state. These H-bonds enhance the crystallinity and dramatically increase the inter-laminar space of the crystalline zone, reducing the interchain free space and increasing the interaction between amorphous and crystalline regions, making it more mechanically resistive and therefore more stable. Moreover, the strong inter/intramolecular forces in the short range (electrostatic forces) and large range (dispersion forces) also play an important role in the interactions. The surface properties and the degree of swelling can therefore all be tuned via the adjustment of the pH.

■ ASSOCIATED CONTENT

Supporting Information

The Supporting Information is available free of charge on the ACS Publications website at DOI: 10.1021/acsomega.7b01307.

Graphical description of the pendant drop method for surface tension measurements; graphical representation of the initial water cluster as droplet; Young's law interpretation as a force balance of surface tension; and force balance (PDF)

■ AUTHOR INFORMATION

Corresponding Author

*E-mail: hagg@ntnu.no. Tel: +47-735-94033. Fax: +47-735-94080.

ORCID

May-Britt Hägg: 0000-0003-4282-4668

Notes

The authors declare no competing financial interest.

■ ACKNOWLEDGMENTS

The GASSNOVA project 229949 highly recognizes contributions from the CLIMIT-Demo program in the Norwegian Research Council, Air Products and Chemicals, Inc., Alberta Innovation (Canada), Statoil AS (Norway), SINTEF Materials and Chemistry and DNV GL (The Netherlands).

■ REFERENCES

(1) Sandru, M. *Development of a FSC Membrane for Selective CO_2 Capture*; Norwegian University of Science and Technology, Faculty of Natural Sciences and Technology, Department of Chemical Engineering: Trondheim, 2009.

(2) Chen, X.; Wang, Y.; Pelton, R. pH-Dependence of the Properties of Hydrophobically Modified Polyvinylamine. *Langmuir* **2005**, *21*, 11673−11677.

(3) Mathur, A. M.; Drescher, B.; Scranton, A. B.; Klier, J. Polymeric emulsifiers based on reversible formation of hydrophobic units. *Nature* **1998**, *392*, 367−370.

(4) Drescher, B.; Scranton, A. B.; Klier, J. Synthesis and characterization of polymeric emulsifiers containing reversible hydrophobes: poly(methacrylic acid-g-ethylene glycol). *Polymer* **2001**, *42*, 49−58.

(5) Chen, G.; Hoffman, A. S. Graft copolymers that exhibit temperature-induced phase transitions over a wide range of pH. *Nature* **1995**, *373*, 49−52.

(6) Suwa, K.; Morishita, K.; Kishida, A.; Akashi, M. Synthesis and functionalities of poly(N-vinylalkylamide). V. Control of a lower critical solution temperature of poly(N-vinylalkylamide). *J. Polym. Sci., Part A: Polym. Chem.* **1997**, *35*, 3087−3094.

(7) Suwa, K.; Wada, Y.; Kikunaga, Y.; Morishita, K.; Kishida, A.; Akashi, M. Synthesis and functionalities of poly(N-vinylalkylamide). IV. Synthesis and free radical polymerization of N-vinylisobutyramide and thermosensitive properties of the polymer. *J. Polym. Sci., Part A: Polym. Chem.* **1997**, *35*, 1763−1768.

(8) Kim, T.-J.; Li, B.; Hägg, M.-B. Novel fixed-site-carrier polyvinylamine membrane for carbon dioxide capture. *J. Polym. Sci., Part B: Polym. Phys.* **2004**, *42*, 4326−4336.

(9) Vendra, V. K.; Wu, L.; Krishnan, S. Polymer Thin Films for Biomedical Applications. In *Nanotechnologies for the Life Sciences*; Wiley-VCH Verlag GmbH & Co. KGaA, 2007.

(10) Nebel, R. L.; Saacke, R. G. Technology and applications for encapsulated spermatozoa. *Biotechnol. Adv.* **1994**, *12*, 41−48.

(11) Shi, L.; Berkland, C. Acid-Labile Polyvinylamine Micro- and Nanogel Capsules. *Macromolecules* **2007**, *40*, 4635−4643.

(12) Pinschmidt, R. K.; Lai, T. W. Enhanced Oil Recovery with High Molecular Weight Polyvinylamine Formed in Situ. Google Patents, 1990.

(13) Deng, L.; Kim, T.-J.; Hägg, M.-B. PVA/PVAm blend FSC membrane for CO2-capture. *Desalination* **2006**, *199*, 523−524.

DOI: 10.1021/acsomega.7b01307
ACS Omega 2017, 2, 8388−8400

(14) Deng, L.; Kim, T.-J.; Hägg, M.-B. Facilitated transport of CO2 in novel PVAm/PVA blend membrane. *J. Membr. Sci.* **2009**, *340*, 154−163.
(15) Deng, L.; Kim, T.-J.; Sandru, M.; Hägg, M.-B. In *PVA/PVAm Blend FSC Membrane for Natural Gas Sweetening A2 - Alfadala, Hassan E*, Proceedings of the 1st Annual Gas Processing Symposium; Reklaitis, G. V. R., El-Halwagi, M. M., Eds.; Elsevier: Amsterdam, 2009; Vol. 1; pp 247−255.
(16) Deng, L.; Hägg, M.-B. Techno-economic evaluation of biogas upgrading process using CO2 facilitated transport membrane. *Int. J. Greenhouse Gas Control* **2010**, *4*, 638−646.
(17) Deng, L.; Hägg, M.-B. Swelling behavior and gas permeation performance of PVAm/PVA blend FSC membrane. *J. Membr. Sci.* **2010**, *363*, 295−301.
(18) Hussain, A.; Hägg, M.-B. A feasibility study of CO2 capture from flue gas by a facilitated transport membrane. *J. Membr. Sci.* **2010**, *359*, 140−148.
(19) Kim, T.-J.; Uddin, M. W.; Sandru, M.; Hägg, M.-B. The effect of contaminants on the composite membranes for CO2 separation and challenges in up-scaling of the membranes. *Energy Procedia* **2011**, *4*, 737−744.
(20) Uddin, M. W.; Hägg, M.-B. Natural gas sweetening-the effect on CO2−CH4 separation after exposing a facilitated transport membrane to hydrogen sulfide and higher hydrocarbons. *J. Membr. Sci.* **2012**, *423−424*, 143−149.
(21) Uddin, M. W.; Hägg, M.-B. Effect of monoethylene glycol and triethylene glycol contamination on CO2/CH4 separation of a facilitated transport membrane for natural gas sweetening. *J. Membr. Sci.* **2012**, *423−424*, 150−158.
(22) Kim, T.-J.; Vrålstad, H.; Sandru, M.; Hägg, M.-B. Separation performance of PVAm composite membrane for CO2 capture at various pH levels. *J. Membr. Sci.* **2013**, *428*, 218−224.
(23) Kim, T.-J.; Vrålstad, H.; Sandru, M.; Hägg, M.-B. The effect of pH on CO2-separation from post combustion gas by polyvinylamine based composite membrane. *Energy Procedia* **2013**, *37*, 986−992.
(24) He, X.; Hägg, M.-B. Energy Efficient Process for CO2 Capture from Flue gas with Novel Fixed-site-carrier Membranes. *Energy Procedia* **2014**, *63*, 174−185.
(25) He, X.; Kim, T.-J.; Hägg, M.-B. Hybrid fixed-site-carrier membranes for CO2 removal from high pressure natural gas: Membrane optimization and process condition investigation. *J. Membr. Sci.* **2014**, *470*, 266−274.
(26) Sandru, M.; Kim, T.-J.; Hägg, M.-B. High molecular fixed-site-carrier PVAm membrane for CO2 capture. *Desalination* **2009**, *240*, 298−300.
(27) Sandru, M.; Haukebø, S. H.; Hägg, M.-B. Composite hollow fiber membranes for CO2 capture. *J. Membr. Sci.* **2010**, *346*, 172−186.
(28) Zhao, H. C.; Li, Q.; Bai, L. B.; Huang, F. Study on Glass Transition Temperature of Polyvinylamine Hydrochloride. *Adv. Mater. Res.* **2011**, *217−218*, 1066−1069.
(29) Nieto, D. R.; Santese, F.; Toth, R.; Posocco, P.; Pricl, S.; Fermeglia, M. Simple, Fast, and Accurate In silico Estimations of Contact Angle, Surface Tension, and Work of Adhesion of Water and Oil Nanodroplets on Amorphous Polypropylene Surfaces. *ACS Appl. Mater. Interfaces* **2012**, *4*, 2855−2859.
(30) He, X.; Romero-Nieto, D.; Lindbråthen, A.; Hägg, M.-B. Membrane System for CO2 Capture: From Molecular Modelling to Process Simulation. In *Process Systems and Materials for CO2 Capture: Modelling, Design, Control*; Athanasios, I., Papadopoulos, P. S., Eds.; John Wiley Sons, Inc.: U.K., 2017; pp 249−282.
(31) Hagler, A. T.; Lifson, S.; Dauber, P. Consistent force field studies of intermolecular forces in hydrogen-bonded crystals. 2. A benchmark for the objective comparison of alternative force fields. *J. Am. Chem. Soc.* **1979**, *101*, 5122−5130.
(32) Sun, H.; Mumby, S. J.; Maple, J. R.; Hagler, A. T. An ab Initio CFF93 All-Atom Force Field for Polycarbonates. *J. Am. Chem. Soc.* **1994**, *116*, 2978−2987.
(33) Sun, H. COMPASS: An ab Initio Force-Field Optimized for Condensed-Phase ApplicationsOverview with Details on Alkane and Benzene Compounds. *J. Phys. Chem. B* **1998**, *102*, 7338−7364.
(34) Rigby, D.; Sun, H.; Eichinger, B. E. Computer simulations of poly(ethylene oxide): force field, pvt diagram and cyclization behaviour. *Polym. Int.* **1997**, *44*, 311−330.
(35) Yang, J.; Ren, Y.; Tian, A.-m.; Sun, H. COMPASS Force Field for 14 Inorganic Molecules, He, Ne, Ar, Kr, Xe, H2, O2, N2, NO, CO, CO2, NO2, CS2, and SO2, in Liquid Phases. *J. Phys. Chem. B* **2000**, *104*, 4951−4957.
(36) Berendsen, H. J. C.; Grigera, J. R.; Straatsma, T. P. The missing term in effective pair potentials. *J. Phys. Chem.* **1987**, *91*, 6269−6271.
(37) Plazzer, M. B.; Henry, D. J.; Yiapanis, G.; Yarovsky, I. Comparative Study of Commonly Used Molecular Dynamics Force Fields for Modeling Organic Monolayers on Water. *J. Phys. Chem. B* **2011**, *115*, 3964−3971.
(38) Rigby, D. Fluid density predictions using the COMPASS force field. *Fluid Phase Equilib.* **2004**, *217*, 77−87.
(39) Heinz, H.; Vaia, R. A.; Farmer, B. L.; Naik, R. R. Accurate Simulation of Surfaces and Interfaces of Face-Centered Cubic Metals Using 12-6 and 9-6 Lennard-Jones Potentials. *J. Phys. Chem. C* **2008**, *112*, 17281−17290.
(40) Lee, W.-J.; Ju, S.-P. Dynamical Property of Water Droplets of Different Sizes Adsorbed onto a Poly(methyl methacrylate) Surface. *Langmuir* **2010**, *26*, 438−446.
(41) Darden, T.; York, D.; Pedersen, L. Particle mesh Ewald: An N·log(N) method for Ewald sums in large systems. *J. Chem. Phys.* **1993**, *98*, 10089−10092.
(42) Manias, E.; Kuppa, V. The origins of fast segmental dynamics in 2 nm thin confined polymer films. *Eur. Phys. J. E: Soft Matter* **2002**, *8*, 193−199.
(43) Fermeglia, M.; Pricl, S. Equation-of-state parameters for pure polymers by molecular dynamics simulations. *AIChE J.* **1999**, *45*, 2619−2627.
(44) Theodorou, D. N.; Suter, U. W. Detailed molecular structure of a vinyl polymer glass. *Macromolecules* **1985**, *18*, 1467−1478.
(45) Flory, P. J. *Principles of Polymer Chemistry*, 1st ed.; Cornell University Press: Ithaca, 1953; p 688.
(46) Andrea, T. A.; Swope, W. C.; Andersen, H. C. The role of long ranged forces in determining the structure and properties of liquid water). *J. Chem. Phys.* **1983**, *79*, 4576.
(47) Berendsen, H. J. C.; Postma, J. P. M.; van Gunsteren, W. F.; DiNola, A.; Haak, J. R. Molecular dynamics with coupling to an external bath. *J. Chem. Phys.* **1984**, *81*, 3684.
(48) Valleaou, J. P. In *The Problem of Long-range Forces in the Computer Simulation of Condensed Media*, NRCC, Workshop Proceedings 1980; Ceperley, D., Ed., 1980; p 3.
(49) Das, S.; Marchand, A.; Andreotti, B.; Snoeijer, J. H. Elastic deformation due to tangential capillary forces. *Phys. Fluids* **2011**, *23*, No. 072006.
(50) Finn, R. The contact angle in capillarity. *Phys. Fluids* **2006**, *18*, No. 047102.
(51) Finn, R. Comments related to my paper "The contact angle in capillarity". *Phys. Fluids* **2008**, *20*, No. 107104.
(52) Marchand, A.; Weijs, J. H.; Snoeijer, J. H.; Andreotti, B. Why is surface tension a force parallel to the interface? *Am. J. Phys.* **2011**, *79*, 999−1008.
(53) Schrader, M. E. Young-Dupre Revisited. *Langmuir* **1995**, *11*, 3585−3589.
(54) Amiri, M. T.; Amiri, M. C. Comment on "Influence of Microwaves on the Water Surface Tension". *Langmuir* **2015**, *31*, 10931−10932.
(55) Sumaru, K.; Matsuoka, H.; Yamaoka, H. Exact Evaluation of Characteristic Protonation of Poly(vinylamine) in Aqueous Solution. *J. Phys.Chem.* **1996**, *100*, 9000−9005.
(56) Illergård, J.; Wågberg, L.; Ek, M. Bacterial-growth inhibiting properties of multilayers formed with modified polyvinylamine. *Colloids Surf., B* **2011**, *88*, 115−120.

DOI: 10.1021/acsomega.7b01307
ACS Omega 2017, 2, 8388−8400

(57) Hong, J.; Pelton, R. The surface tension of aqueous polyvinylamine and copolymers with N-vinylformamide. *Colloid Polym. Sci.* **2002**, *280*, 203−205.
(58) Zhu, J.; Gosen, C.; Marchant, R. E. Synthesis and characterization of poly(vinyl amine)-based amphiphilic comb-like dextran glycopolymers by a two-step method. *J. Polym. Sci., Part A: Polym. Chem.* **2006**, *44*, 192−199.
(59) Fermeglia, M.; Pricl, S. Multiscale molecular modeling in nanostructured material design and process system engineering. *Comput. Chem. Eng.* **2009**, *33*, 1701−1710.
(60) Ping, Z. H.; Nguyen, Q. T.; Chen, S. M.; Zhou, J. Q.; Ding, Y. D. States of water in different hydrophilic polymers - DSC and FTIR studies. *Polymer* **2001**, *42*, 8461−8467.

DOI: 10.1021/acsomega.7b01307
ACS Omega 2017, 2, 8388−8400